

CONTROLLING INFLUENCE OF MAGNETIC FIELD ON SOLAR WIND OUTFLOW: AN INVESTIGATION USING CURRENT SHEET SOURCE SURFACE MODEL

Bala Poduval

Space Science Institute, Boulder, CO 80303 USA

OBJECTIVES

- Obtain coronal sources of solar wind observed near the Earth's orbit (inverse mapping).
- Obtain their photospheric footpoints by tracing them back along open magnetic field lines (using CSSS and PFSS models).
- Compute flux tube expansion factors (FTE) at each of these points at $2.5 R_{\odot}$.
- Obtain the functional form of the dependence of solar wind speed (SWS) on FTE (fit a quadratic equation).
- Use this fitted quadratic function to predict SWS.
- Deduce the temporal variation, if any, of this functional dependence, i. e., variation of the coefficients of fitted quadratic equation.

INVERSE MAPPING

Solar wind observed by near-Earth spacecraft were mapped back to the source surface along the Archimedian spiral using the set of equations:

$$\Phi_0 = \Phi_R + \frac{R\Omega}{V_R} \quad \text{and} \quad \Theta_0 = \Theta_R \quad (1)$$

Φ_0 , Φ_R : longitudes, & Θ_0 and Θ_R latitudes on source surface and at a distance R from the Sun; Ω : angular velocity of solar rotation; V_R : observed SWS. This procedure assumes: (1) Solar wind outflow is radial. (2) Interaction between slow and fast wind streams between Sun and Earth is negligible. Following the argument of Poduval & Zhao (JGR, 109, 2004), we used the daily averaged solar wind speed for this inverse mapping.

DATA

Period of Study: Solar cycles 23 and early 24 (two years) 1996 – 2010 (CRs 1912 – 2103).

- Observed solar wind data: Multispacecraft compilation of near-Earth solar wind observations: <http://omniweb.gsfc.nasa.gov/>.
- Photospheric Synoptic Maps: MDI, WSO, MWO, SOLIS Phase P1: 1996–1998 (CRs 1912–1936); studied earlier, Paper I Poduval & Zhao, ApJ Letters, 782, L22. Phase P2: 1999–2001 (CRs 1947–1985); ascending–maximum of solar cycle 23. Phase P3: 2008–2010 (CRs 2073–2092); early ascending phase of solar cycle 24. Missing: CRs1937–1946; 2086 (MDI); CRs2089-2091 (MWO).

QUADRATIC FIT

Note that the lowest value of $\log(\text{FTE})$ during Phase P3 is 0.8 which implies (as inferred from Table 1) SWS above 650 km s^{-1} may not be predicted accurately. The high values ($> 950 \text{ km s}^{-1}$) of the y -intercept (c) seem to support this. During Phase P2, values as low as 0.4 are present and c seldom exceed 950 km s^{-1} (except during 1950–1952 where it is 1029 km s^{-1}). The maximum values of $\log(\text{FTE})$ are also different during the two phases P2 and P3, but values between 1.3 and 2.0 (as in P3) is sufficient to predict most of the observed slow wind.

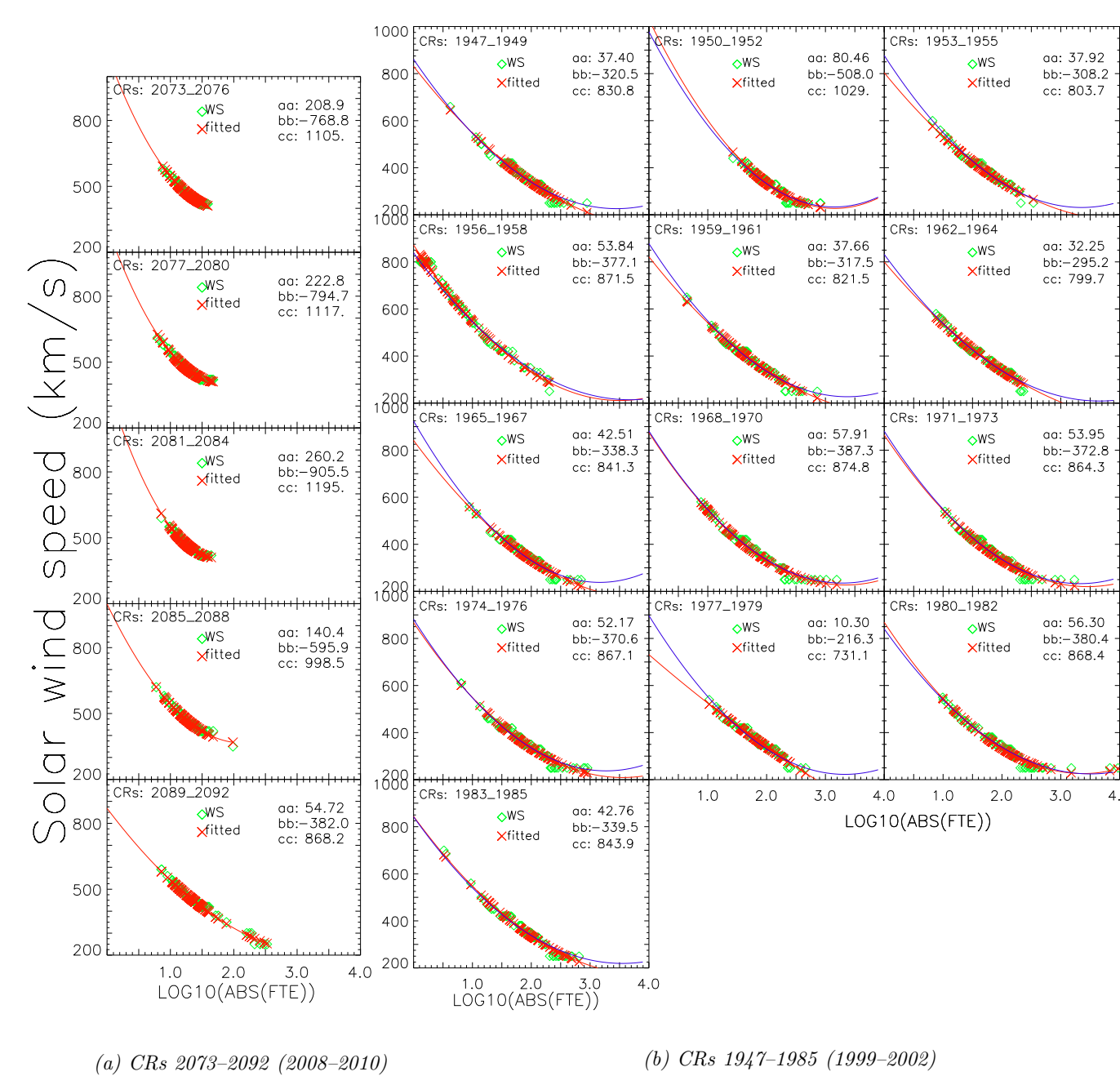


Figure 1 The best-fit quadratic function to $\log(\text{FTE})$ -SWS for CSSS model (red lines) computed with MDI synoptic maps. The WS predictions are represented by 'x' while the 'o' and the solid line depict the fitted curve. The coefficients a , b and c , of the fitted quadratic functions are given at the top, right-hand corner in each panel. Panel (a) represents Phase P3, while Panel (b) depicts Phase P2. The blue curves in Panel (b) represent the PFSS model.

BACKGROUND

Flux Tube Expansion factor (FTE) is the rate at which the magnetic flux tubes expand between photosphere and a source surface higher up in the corona. Mathematically,

$$\text{FTE} = \left(\frac{R_{\odot}}{R_{ss}} \right)^2 \frac{B(\text{phot})}{B(ss)} \quad (2)$$

$B(\text{phot})$; $B(ss)$: photospheric and source surface magnetic fields at radii R_{\odot} and R_{ss} . Wang & Sheeley (ApJ, 355, 726, 1990) obtained an empirical inverse relationship between SWS and FTE using the PFSS model (Table 1). This inverse relation implies that both slow and fast solar wind arise from coronal holes: Fast wind from the centers and slow wind from the boundaries. This forms the basis of state-of-the-art solar wind prediction technique – the WSA model (Arge & Pizzo, JGR, 105, 10,465, 2000).

Table 1 WS RELATION

SWS	> 750	650–750	550–650	450–550	< 450
FTE	< 4.5	4.5–8.0	8.0–10.0	10.0–20.0	> 20.0

QUADRATIC FUNCTION

We mapped the solar wind observed near the Earth's orbit during 1996–2010 back to the source surface (at $15 R_{\odot}$ in CSSS model and $2.5 R_{\odot}$ in PFSS model) and obtained the location of their coronal source. By mapping these back on to the photosphere we determined their photospheric footpoints and computed FTEs for the entire period of study.

We fitted a curve of the form:

$$\text{SWS} = a * (\log(\text{FTE}))^2 + b * (\log(\text{FTE})) + c \quad (3)$$

to the pair of computed FTEs and the observed SWS, based on the WS relationship between the two as given in Table 1. The fitted curves for CSSS model for Phases P2 and P3 are depicted in Figure 1. The shapes of the curves change from near parabolic to almost a straight line. Also, the ranges of FTEs vary significantly during the two phases. The coefficients a , b and c , obtained for the two models are plotted in Figure 2 for the entire period of study using MDI data (left panels LP) and for Phase P3 using SOLIS, WSO and MWO synoptic maps.

INFLUENCE OF MAGNETIC FIELD ON SOLAR WIND OUTFLOW

The electric currents in the lower corona manifest themselves as the many structures seen in coronal images (A. J. Hundhausen 1972: Coronal Expansion and Solar Wind). At some height in the coronal atmosphere, around $2.5 R_{\odot}$, the source surface location in CSSS model and the cusp surface in PFSS models, closed field configurations are no longer found and all the field lines are open, with a current sheet at the polarity inversion region. Beyond this height, the solar wind controls the magnetic field, carrying it into the heliosphere to form HMF (E. N. Parker, ApJ, 128, 664, 1958). This interplay between the magnetic field and the solar wind at the base of the corona is likely to be reflected in the spatial and temporal variations of FTE, which obviously is controlled by magnetic fields. The spatial variations of FTEs are incorporated into the well known Wang and Sheeley empirical relationship. This poster presents the results of an investigation of the temporal variations of FTE-SWS relationship and, thereby, attempts to infer the controlling influence of the coronal magnetic field in determining the solar wind outflow.

We used Current Sheet Source surface (CSSS) model to obtain coronal sources and their photospheric footpoints of the solar wind observed near Earth, and to compute FTEs. The model was developed by Zhao & Hoeksema (JGR, 100, 19, 1995) based on the analytical solutions for the magnetic field and current density obtained by Bogdan and Low (ApJ, 306, 271, 1986) for a corona in static equilibrium. The CSSS model incorporates volume and sheet currents, and a source surface that can have a variable location. The geometry of CSSS model is depicted in Figure 3.

We carried out the work using synoptic maps from MDI, WSO, MWO and SOLIS. We made a comparison with the results obtained with Potential Field Source Surface (PFSS) model, adopting the same procedures.

GEOMETRY OF CSSS MODEL

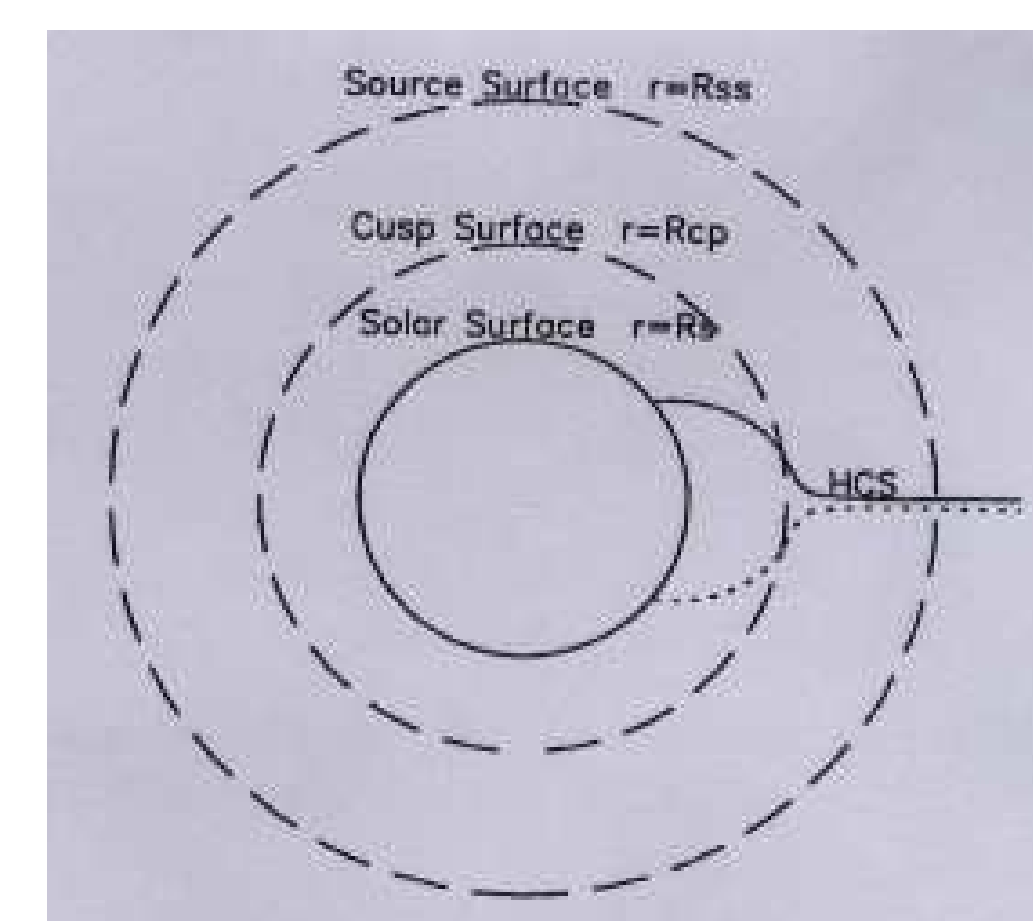


Figure 2: The cusp surface R_{cp} , representing the locus of cusp points of helmet streamers, was placed at $2.5 R_{\odot}$. The source surface R_{ss} , free to be placed anywhere outside cusp surface, was placed at $15 R_{\odot}$.

ANOMALOUS BEHAVIOR OF FITTED COEFFICIENTS

Note the dramatic difference in the behaviour of the fitted coefficients during Phase P3. The difference is most significant for CSSS model and for MDI synoptic maps. There is little variation for the PFSS model during Phase P3, whereas the variation is comparable to that of CSSS model during most other periods. Also, note the similar, but less dramatic, variations exhibited by other synoptic maps.

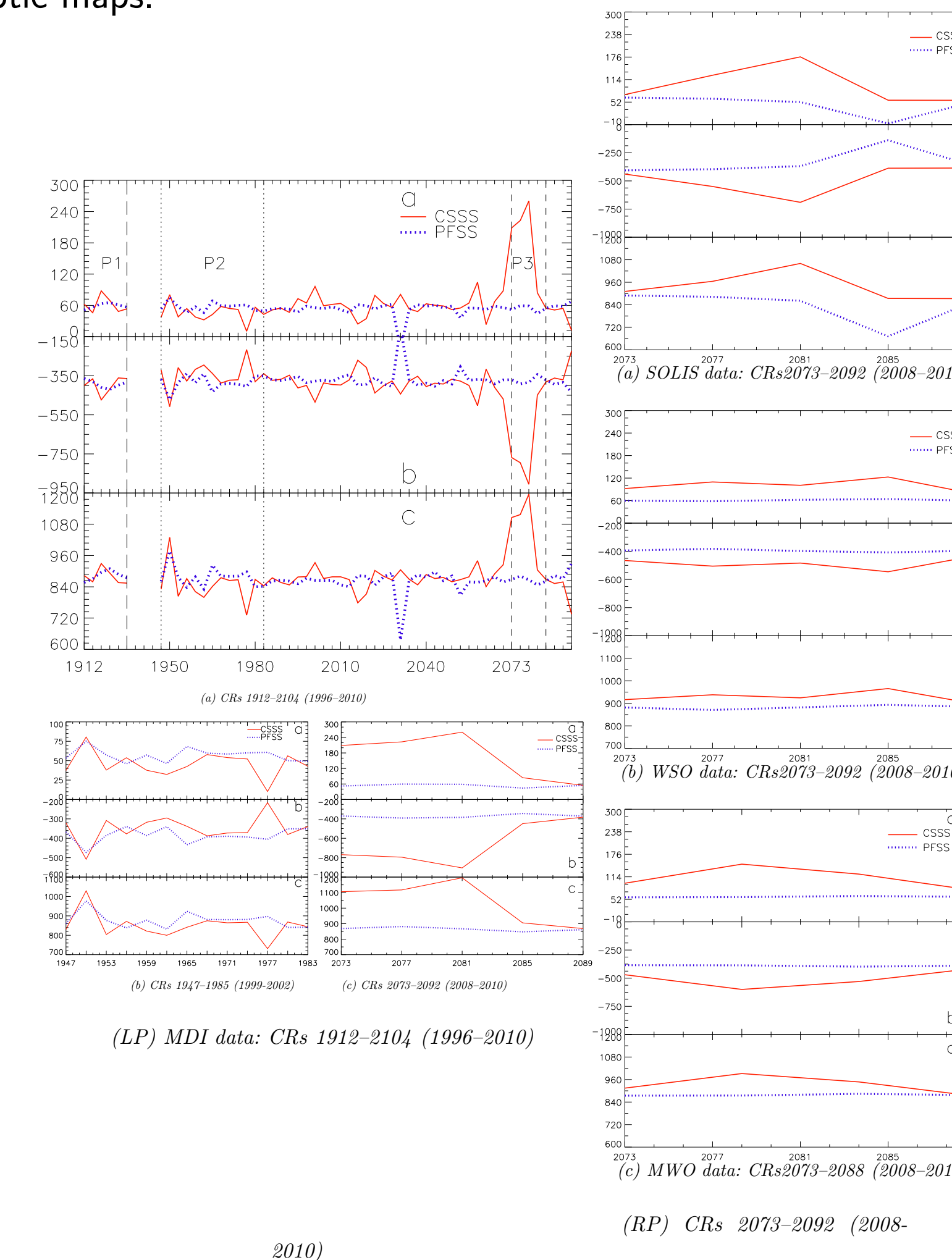


Figure 3 The temporal variations of the coefficients a , b and c of the best-fit quadratic equations obtained for CSSS (red) and PFSS (blue) models. Left panels (LP) depict MDI data where Panel (a) includes the entire period of study, Panel (b) shows Phase P2 and Panel (c) represents Phase P3. Right panels (RP) are similar to Panel (c) on LP but for SOLIS (panel (a)), WSO (panel (b)), and MWO (panel (c)).

METRIC OF ACCURACY

We obtained the correlation coefficients and the RMS errors between observed and predicted solar wind speeds for the two models. Also, we determined the ratios of the RMS errors:

$$\text{RMSE RATIO} = \text{RMSE}_{\text{PFSS}} / \text{RMSE}_{\text{CSSS}} \quad (4)$$

Based on the arguments in Paper I, we took the RMSE RATIO as a metric of accuracy in determining the performances of the two models. Figure 5 depicts the RMSE ratio, the RMS errors and the correlation coefficients for Phase P3. As clear from the figure, the CSSS predictions for this period of study are significantly better than those of PFSS model; for the CSSS model, the RMS error is much smaller and the correlation coefficients significantly greater than those for PFSS model.

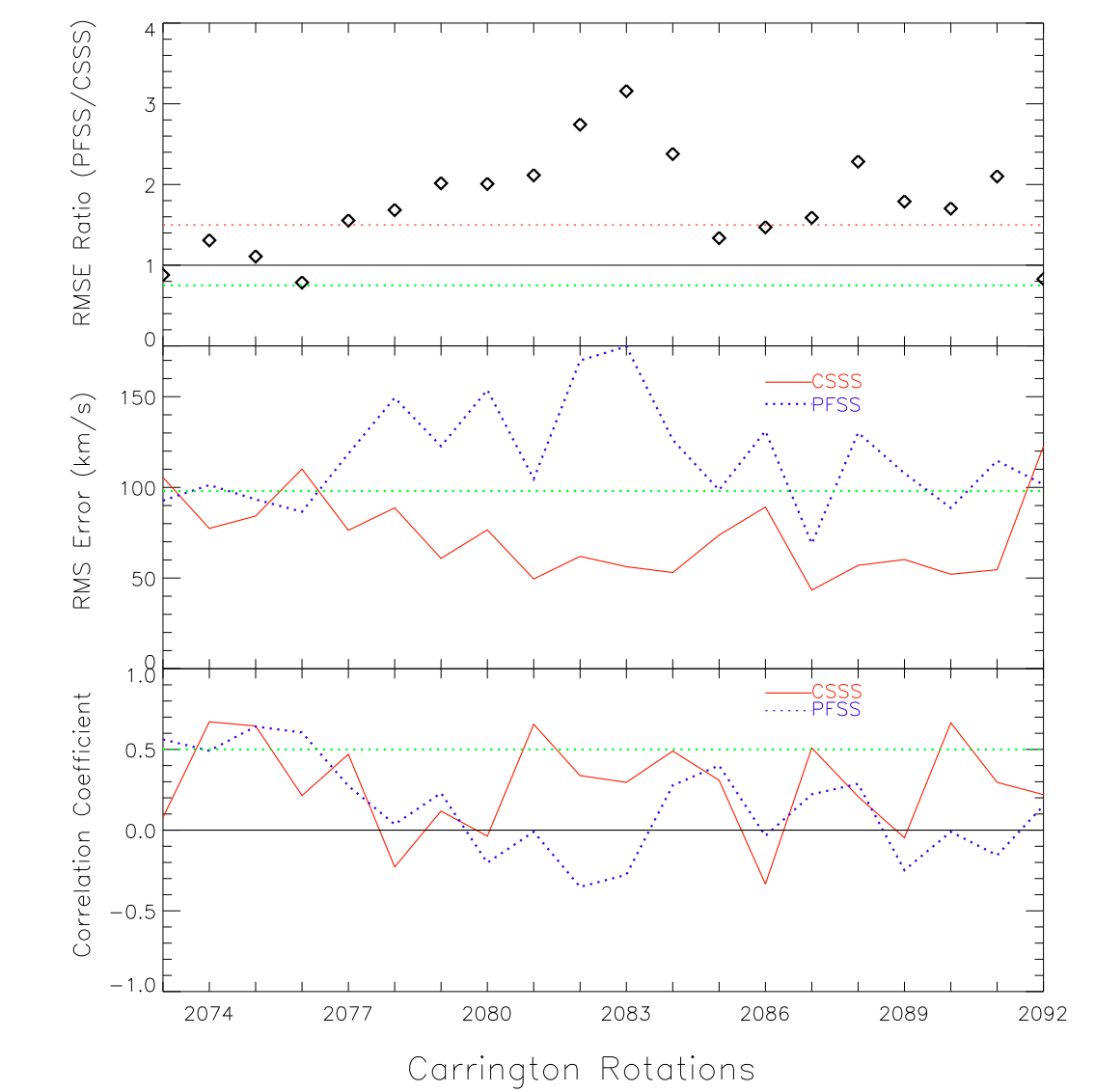


Figure 5: RMS ratio (Eq 4, (top panel); and RMS errors (middle panel) and correlation coefficients (bottom panel) between observed solar wind and those predicted by CSSS (red) and PFSS (blue) models.

Summary & Conclusion

- We notice an anomaly in the temporal variations of the coefficients of the fitted quadratic equation during Phase P3 in the case of CSSS model, particularly using MDI synoptic maps. Similar, but less dramatic, variations exhibited by other synoptic maps confirm that this must be related to the characteristics of magnetic field during this period, 2008-early 2010 (solar cycle 24). Being a period of extended minimum (and quite unusual), such an anomalous behavior is scientifically intriguing and worth exploring further.
- If the anomalous behavior is real, then this investigation suggests that CSSS model captures subtle characteristics of the solar magnetic field and reflects them in the predicted solar wind. A detailed investigation, including optimization of the free parameters of the CSSS model is currently underway.
- Moreover, the more dramatic changes in the case of MDI might be due to the differences (limitations) in the polar field correction techniques applied by different observatories.
- The magnetic neutral lines computed using CSSS model with different synoptic maps approximately agree with each other. Though there is a large difference in the latitudinal extents of neutral lines computed using CSSS and PFSS models, a point worthy of note is that the sector boundary crossings are rather consistent.
- CSSS model predicts the solar wind speed nearly twice better than PFSS model.
- The better accuracy is attributed to the particular geometry and more accurate scenario of the corona modeled in CSSS model.

Acknowledgements

Drs. X. -P. Khao, Y. -M. Wang, J. T. Hoeksema and Prof. P. H. Scherrer are gratefully acknowledged for the various supports, discussions and suggestions. Mount Wilson data made available by Dr. Y.-M. Wang. SOHO is a project of international cooperation between ESA and NASA. Data were acquired by SOLIS instruments operated by NISP/NSO/AURA/NSF. WSO data by courtesy of Dr. J. T. Hoeksema

Acronyms

WS	Wang & Sheeley	MWO	Mount Wilson Observatory
FTE	flux tube expansion	WSO	Wilcox Solar Observatory
SWS	solar wind speed	MDI	Michelson Doppler Imager
RMSE	root mean square error	SOLIS	Synoptic Optical Long-term Investigations of the Sun

NEUTRAL LINES

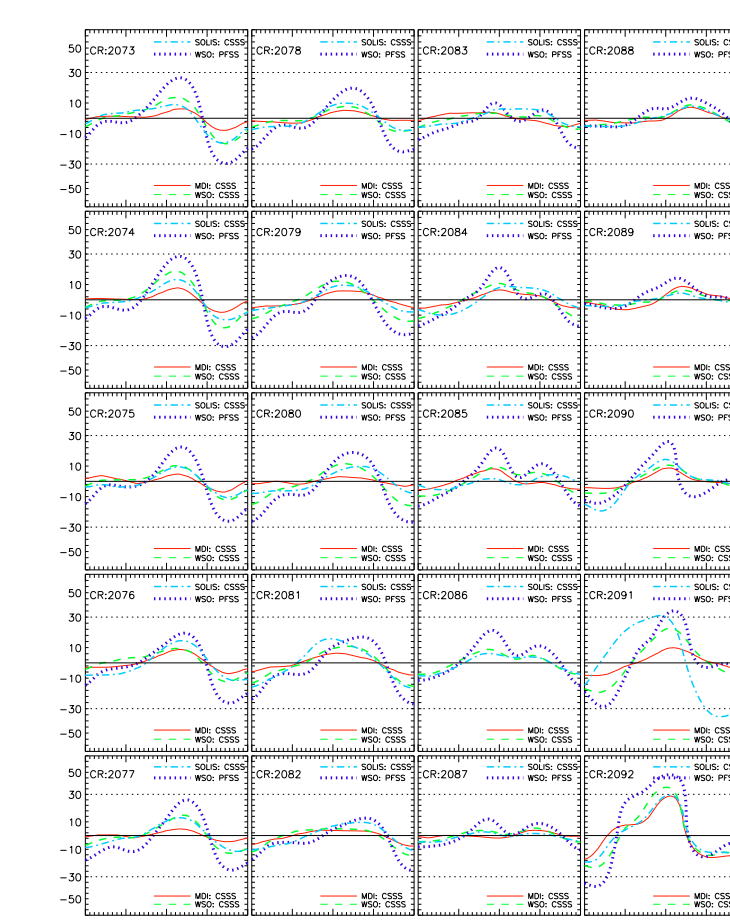


Figure 4 Comparison of neutral lines computed using CSSS model and MDI (red line), WSO (green dashed lines) and SOLIS synoptic maps (light blue dot-dashed lines). Also plotted are the neutral lines obtained using PFSS model (blue dotted lines) and WSO synoptic maps (taken from the WSO website: courtesy Dr. J. T. Hoeksema). The MDI data for CR 2086 contains data gaps and therefore, excluded from the study.